文章编号：1001-9014(2021)06-0715-06

DOI:10.11972/j.issn.1001-9014.2021.06.002

InAlAs/InGaAs avalanche photodiode with an optimized multiplication layer

GU Yu-Qiang[1,2], TAN Ming[2], WU Yuan-Yuan[2], LU Jian-Ya[2], LI Xue-Fei[1,2], LU Shu-Long[2*]

(1. Institute of Nano-Tech and Nano-Bionics, University of Science and Technology of China, Hefei 230026, China;
2. Key Laboratory of Nano-devices and Applications, Suzhou Institute of Nano-Tech and Nano-Bionics, Chinese Academy of Sciences, Suzhou 215123, China)

Abstract: In this paper, the trade-off between gain-bandwidth product (GBP) and dark current of an InAlAs/InGaAs avalanche photodiode (APD) was studied by optimizing multiplication layer. An optimized multiplication layer with 200 nm was proposed to improve the GBP and reduce the dark current. The fabricated InAlAs/InGaAs APD shows an excellent performance which is consistent with the calculated results. A high responsivity of 0.85 A/W (M=1) at 1.55 μm and a high GBP of 155 GHz was achieved, whereas the dark current is as low as 19 nA at 0.9 V_b. This study is significant to the future high-speed transmission application of the avalanche photodiodes.

Key words: avalanche photodiodes (APDs), gain-bandwidth product (GBP), dark current
PACS: 85.60.Bt, 85.60.Dw

具有优化倍增层 InAlAs / InGaAs 雪崩光电二极管

顾宇强[1,2], 谭 明[2], 吴渊渊[2], 卢建娅[2], 李雪飞[1,2], 陆书龙[2*]

(1. 中国科学技术大学 纳米技术与纳米仿生学院,安徽 合肥 230026;
2. 中国科学院苏州纳米技术与纳米仿生研究所 纳米器件与应用重点实验室,江苏 苏州 215123)

摘要:通过优化倍增层的厚度,研究了InAlAs/InGaAs雪崩光电二极管增益带宽积和暗电流之间的关系。利用仿真计算得出200 nm厚的倍增层能够改善增益带宽积并降低暗电流。制成的InAlAs/InGaAs雪崩光电二极管性能优异,与计算趋势一致。在获得0.85 A/W的高响应和155 GHz的增益带宽积的同时,器件暗电流低于19 nA。这项研究对雪崩光电二极管在未来高速传输的应用具有重要意义。

关 键 词:雪崩光电二极管;增益带宽积;暗电流

中图分类号:O436　　**文献标识码**:A

Introduction

Over the past decades, avalanche photodiodes (APDs) have been widely used for commercial, military and scientific research[1]. The application of optical communications [2], imaging [3-4] and single photo detection [5-6] has always been the main driving force for the sustainable development of APD. APD with InP as the multiplication layer and $In_{0.53}Ga_{0.47}As$ (InGaAs) as the absorption layer has been studied for a long time[7-8]. In contrast to InP, InAlAs has a better ionization coefficient ratio (k=0.15~0.3 [9]) than that of InP (k=0.4~0.5 [10]), which leads to both higher sensitivity and lower noise. Moreover, the band gap of InAlAs is slightly larger than that of InP, the tunnel current is expected to be smaller.

Gain-bandwidth product (GBP) is an important characteristic of APDs for application in high-speed transmission, however, a device with high GBP often results in a high dark current, which is closely related to the thickness of the multiplication layer. M. Nada *et al.* reported that an APD device with a higher bandwidth in the case of a thinner multiplication layer was obtained. However, the dark current of the device will also increase with decreasing multiplication layer [11]. This phenomenon lies in the fact that when the avalanche occurs

Received date: 2021-04-09, **revised date**: 2021-09-28　　**收稿日期**:2021-04-09,**修回日期**:2021-09-28

Foundation items: Supported by the National High Technology Research and Development Program of China (2018YFB2003305), the Key R&D Program of Jiangsu Province (BE2018005), the Science and Technology Service Network Initiative of the Chinese Academy of Sciences (KFJ-STS-ZDTP-086), the Support From SINANO (Y8AAQ11003), Natural Science Foundation of Jiangsu Province (BK20180252)

Foundation items: GU Yu-Qiang (1995-), male, Taizhou China. Master, Research area focus on performance simulation and process preparation of avalanche photodiode. E-mail: yqgu2019@sinano.ac.cn

* **Corresponding author**: E-mail: sllu2008@sinano.ac.cn

in the thin multiplication layer, the electric field in the multiplication layer is very high, resulting in a large tunneling dark current. On the contrary, Ferraro *et al.* found that when the thickness of the multiplication layer reaches 400 nm, the dark current is about 10 nA, but the bandwidth is only about 1 GHz [12]. Aims to obtain high bandwidth and low dark current at the same time, we need to adopt the appropriate thickness of the multiplication layer. However, too many parameters in the complicated device make the experiment more difficult. The main motivation of this work is to establish a quantitative and predictive physical model for the operation of APD device. On the basis of the model, a less experimental work will be good enough to obtain a better device performance.

In this paper, we designed a mesa InAlAs/InGaAs APD with an optimized 200 nm InAlAs multiplication layer. The electric field distribution, current-voltage (*I-V*) characteristics, capacitance-voltage (*C-V*) characteristics, gain characteristics and frequency characteristic are calculated by Silvaco Atlas tool. The fabricated InGaAs/InAlAs APD with a diameter of 30 μm exhibits low dark current of 19 nA at 0.9 V_b and high gain-bandwidth product about 155 GHz. The experiment results show a good agreement with the calculation.

1 Device design and calculation

A two-dimensional model of InAlAs/InGaAs separate absorption, grading, charge and multiplication (SAGCM) APD is established on the basis of the calculation of the device by using the Atlas Silvaco. The calculation is based on the drift-diffusion model, the Poisson equation and carrier continuity equation to calculate the electrical and optical performance. In order to make the device calculation results closer to the actual operating mode, the calculation process follows assumptions and simplifications [13]:

1. P^+-N is an abrupt junction
2. The multiplication, charge, grading and absorption layers are uniform doping
3. The absorption layer is completely depleted at punch-through voltage

The physical models used in the calculation including the Shockley-Read-Hall Recombination (SRH), Auger Recombination (AUGER), Optical Radiative Recombination (OPTR) and Impact Ionization Model (IMPACT). In addition, the Fermi-Dirac model is used for the static characteristics of the carrier, and the high field saturation model is used to consider the effect of mobility reduction under high electric field. Ray tracing model is utilized for calculating optical characteristic. Newton's numerical iterative analysis method is used to derive the solutions of Poisson equation and continuity equation. Specific model information can refer to the following literatures[14-16]. Table 1 lists some of the material parameters used in the calculation [16-18].

Figure 1 shows the cross-sectional view of the InAlAs/InGaAs (SAGCM) APD. The semi-insulating InP substrate is followed by an N-type doped InP buffer layer and an N-type $In_{0.52}Al_{0.48}As$ layer. The intrinsic multiplication layer $In_{0.52}Al_{0.48}As$ is under the P-type doped $In_{0.52}Al_{0.48}As$ charge layer, and the P-type doped $In_{0.52}Al_{0.48}As$ charge layer has a doping concentration of 4×10^{17}. The thickness of the multiplication layer is optimized to maximize the gain bandwidth product and reduce the dark current. The function of the charge layer is to adjust the electric field distribution of the device. The undoped InAlGaAs grading layer which is used to prevent carrier pile up at the heterointerface between InGaAs and InAlAs. The bandwidth will also be degraded by carrier accumulation at the heterojunction interface[19]. Between the intrinsic $In_{0.53}Ga_{0.47}As$ absorption layer (1.2 μm) and the p-doped InP window layer (1.0 μm), a p-doped InGaAsP grading layer was added. The role of this layer is the same as the InAlGaAs grading layer. Finally a heavily doped P+-$In_{0.53}Ga_{0.47}As$ contact layer helps to reduce the series resistance and to improve the frequency response characteristics of the device.

Table 1 Material parameters used in SILVACO physical modeling
表1 SILVACO仿真中用到的材料参数

Parameters	Units	InGaAs	InAlAs
Band gap	eV	0.75	1.42
Align		0.36	0.36
Permittivity		13.9	12.2
Electron SRH lifetime	s	4×10^{-8}	1×10^{-18}
Hole SRH lifetime	s	4×10^{-8}	1×10^{-18}
Electron mobility	$cm^2/V\cdot s$	10 000	3 000
Hole mobility	$cm^2/V\cdot s$	150	250
Radiative recombination coefficient	cm^3/s	9.6×10^{-1}	1.2×10^{-10}

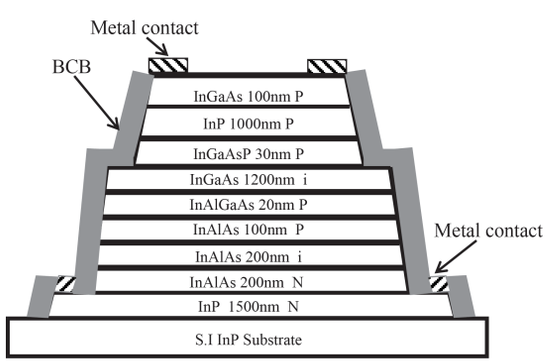

Fig. 1 Structure of InAlAs/InGaAs APD
图1 InAlAs/InGaAs APD的结构图

In APDs, the bandwidth can be expressed as Eq. 1:

$$f_{3-dB} = \frac{1}{2\pi\tau} = \frac{1}{2\pi\sqrt{\tau_{RC}^2 + \tau_t^2 + \tau_a^2}} \quad , \quad (1)$$

where τ is the response time, τ_{RC} is the RC time constant, τ_t is the carrier transit time, τ_a is the avalanche build-up time.

The RC time constant is determined by the depletion region capacitance C, the device series resistance and the load resistance R. As we can see from the Eq. 2:

$$\tau_{RC} = RC = R \cdot \frac{\varepsilon A}{W} \quad , \quad (2)$$

where R is total resistance of the device, C is the depletion region capacitance C, ε is the dielectric constant, A is the PN junction area, W is the width of depletion region.

The transit time includes the following processes: The photo-induced carriers separate in the InGaAs absorption layer and the electrons drift to the InAlAs multiplication layer under the external electric field. Then electron-hole pairs are produced by impact ionization. The electrons transfer to the N metal and the holes transfer to the P metal.

The avalanche build-up time increases when the thickness of multiplication layer decreases. Compared with carry drift time and RC time constant, avalanche multiplication time is dominant. So the thickness of other layers has little effect on GBP because of high gain of APDs. It is very important to design a reasonable thickness of multiplication layer.

The calculated 3-dB bandwidth is shown in Fig. 2, where the inset presents the GBP as a function of the multiplication layer thickness. As the multiplication layer thickness increases, the increased carrier transit time will lead to a low bandwidth and therefore a small GBP. However, the carrier need more time to attain the threshold energy for the impact ionization process when the multiplication layer decreases. This also results in a reduced bandwidth and GBP. According to the above analysis, the optimized multiplication layer thickness is around 0.2 μm.

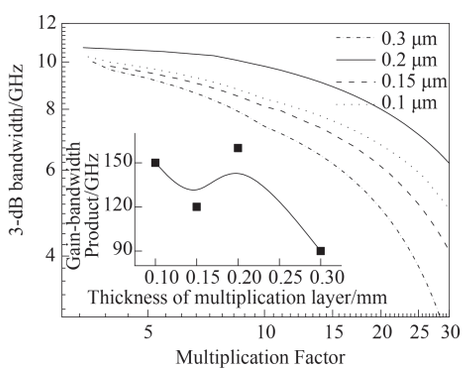

Fig. 2　(a) The 3-dB bandwidth vs multiplication factor with different multiplication layer thickness, and (b) the gain-bandwidth product vs multiplication layer thickness
图2　(a) 3-dB带宽随不同倍增层厚度的变化关系,(b) 增益带宽积和倍增层厚度的关系

The tunneling current is a dominant component of the leakage current at high fields. Tunneling processes include direct band-to-band tunneling (BBT) and trap-assisted tunneling (TAT)[20]. TAT dark current can be neglected when multiplication layer is intrinsic[21]. The BBT dark current density can be expressed as Eq. 3:

$$J_{\text{bbt}} = \frac{\sqrt{2m^*}\, q^3 E^2 W}{4\pi^2 \hbar^2 \sqrt{E_g}} \exp\left(- \frac{4\sqrt{2m^*}\, E_g^{3/2}}{3qE\hbar} \right), \quad (3)$$

where E is the electric field, E_g is the bandgap, m^* is the effective mass and $\hbar$ is the Planck's constant. It can be seen from Eq. 3 that BBT dark current dependents on electric field strength strongly.

Figure 3 shows the calculated electric field distribution with different thicknesses of the multiplication layer. In order to compare the effects of BBT dark currents with different multiplication thickness, the thickness of the other layers remains unchanged except the change of thickness of the multiplication layer. It can be observed that with the increasing thickness of the multiplication layer, the electric filed in the multiplication layer decreases. According to the formula 3, the BBT dark current will decrease. However, with the increase of the multiplication layer thickness, the transit time of the device also increases according to the above analysis, which results in a reduced bandwidth and correspondingly a low gain-bandwidth product. The multiplication layer takes 0.2 μm according to the above analysis.

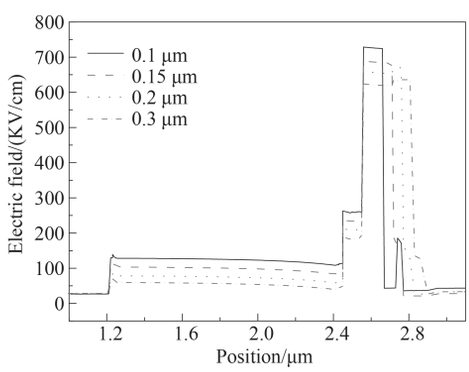

Fig. 3　Distribution of electric field as a function of multiplication layer thickness
图3　不同倍增层厚度的电场强度分布

2　Device fabrication

The device was grown by using Molecular Beam Epitaxy (MBE) on a 350 μm semi-insulating InP substrate. Silicon and beryllium are used as n- and p-doping sources. All epitaxial layers are lattice matched to InP (001) substrate without off-orientation. The growth temperature is 480 ℃, which is monitored by pyrometer. The growth rate is 1um/h. A typical 2×1 reflective high-energy electron diffraction (RHEED) pattern is observed for InGaAs and InGaAsP growth and a 2×4 pattern for InP growth. Doping level in film is confirmed by Hall measurement. The mole fraction is calibrated by beam flux pressure (BEP) and X-ray diffraction (XRD). The actual epitaxial structure is as same as the calculated one. A 1.5 μm n-doped InP buffer layer is followed by a n-doped InAlAs layer. An intrinsic InAlAs multiplication layer (0.2 μm), a p-doped InAlAs charge layer (0.1 μm), a 0.02 μm InAlGaAs grading layer, a 1.2 μm intrinsic absorption layer, a p-doped InGaAsP grading layer (0.03 μm), a p-doped InP layer (1.0 μm) and a 0.1 μm p^+ doped contact layer.

The mesa type APD is fabricated using standard

photolithography, lift-off, wet chemical etching and styrene-acrylic cyclobutene (BCB) passivation. Compared with dry etching, wet etching has less damage to the surface of the device and can reduce surface leakage of the device. Then BCB was coated on the surface of the device and cured at 250 °C for 1 h to form passivation protection on the sidewall of the device. SiNx is selected as the antireflection film, and the active region is formed by lithographically. Finally, the metal is deposited on the anode and cathode.

3 Results and discussion

The measured and calculated dark and photocurrent are shown in Fig. 4 (a). In order to verify the rationality and performance of the device structure, we combined the calculated results and actual test results for analysis. Due to the uncertain factors introduced in the fabrication process, there is a little difference between calculated and actual performance, but both meet the performance requirements. The calculated results have a guiding role in the design and fabrication of the device.

The most important phenomenon to be considered in the calculation of dark current (I_d) is the avalanche process, which is expressed as Eq. 4:

$$I_d = I_{gr} * M + I_t * M^* + I_{du} \quad , \quad (4)$$

among them, I_d is the total dark current, I_{gr} is the generation-recombination current, I_t is the tunneling current which is decided by the electrical field and band gap. I_{du} is the non-multiplied dark current, which is mainly from the surface of the device. M is the multiplication factor of the APD, M^* is the avalanche gain of tunneling dark current.

The calculation of photocurrent (I_p) should consider the generation of electron-hole pairs in the absorption layer and the distribution of electric field both in the charge layer and the multiplication layer. The generation rate of electron-hole pairs produced by impact ionization carriers uses Eq. 5:

$$G = \alpha_n |J|_n + \alpha_p |J|_p \quad , \quad (5)$$

where G is the generation rate of electron-hole pairs, α_n and α_p are the impact ionization coefficients of electrons and holes, respectively. J_n and J_p are the current densities of electrons and holes.

The gain of the device is obtained according to the Eq. 6:

$$M = \frac{I_l - I_d}{I_{l0} - I_{d0}} \quad , \quad (6)$$

M is the multiplication factor , where I_l and I_d are the photocurrent and dark current of the APD, and I_{l0} and I_{d0} are the photocurrent and dark current of the device when M=1.

Under dark condition, no electron-hole pairs are generated and no electrons are injected into the multiplication area. Therefore, the dark current changes little before and after the punch-through voltage (V_p). When the voltage is less than V_p, the photocurrent is close to the dark current. The impact ionization occurs due to carriers are injected into the multiplication layer when bias voltage reaches V_p, which lead to the photocurrent rises. When bias voltage approaches the breakdown voltage (V_b = 28.6 V), the photocurrent rapidly increases to 0.1 mA. In Fig. 4 (a), the calaculated breakdown voltage V_b =-33.6 V (when current reaches 0.1mA), and the actual device breakdown voltage V_p=28.6 V. A high gain of more than 90 can be achieved, and the responsivity at unity gain at 1.55 μm wavelength is 0.85 A/W. The dark current measured at room temperature is 19 nA at 0.9 V_b. The actual measured results of the device are consistent with the calculation trend. No accidental breakdown, such as edge breakdown occurs indicates that our device structure design and fabrication process are reliable. The electric field is effectively limited to the central area. The low surface leakage current can satisfy the applications such as sensitivity receivers. Figure 4 (b) shows the change of gain with reverse bias voltage. After V_p, the gain increases with increasing bias voltage. Under 90% V_b, APD can provide a M>10.

The capacitance-voltage (C-V) characteristic is also particularly important for device structure design and performance evaluation. The actual total capacitance of the SAGCM APD device includes junction capacitance and parasitic capacitance. The parasitic capacitance mainly comes from the metal electrode. The effect of parasitic capacitance is not considered in the calculation process, so the calculated result is smaller than the actual capacitance. The C-V characteristic curve of the device is shown in Fig. 4 (c).

It can be seen from Fig. 4 (c) that the capacitance of the device decreases with the increase of the reverse bias voltage. After reaching the V_p, the capacitance value gradually stabilizes. This indicates that the width of the depletion region of the device becomes wider with the increase of the reverse bias voltage. It can be seen from the Eq. 7:

$$C_j = \frac{\varepsilon_j A}{W} \quad . \quad (7)$$

The width of the depletion region does not change with the reverse bias voltage when the bias voltage greater than V_p, that is, the device is in a completely depleted state. The actual capacitance of the device is 68.7 pF. It can be seen that the calculated and actual V_p are 11.8V and 12.2V respectively, which matches well with value obtained from the I-V characteristics. The bandwidth of the APD detector is closely related to the RC time constant, and the response speed and bandwidth of the device can be improved by reducing the capacitance of the APD.

The frequency response test was analyzed by using a nonlinear vector network analyzer. We measured its frequency response from 20 MHz to 15 GHz at 1550 nm. In order to obtain the theoretical maximum bandwidth, we calculated the 3-dB bandwidth at different voltage. As we can see from Fig. 5, 3-dB bandwidth reaches the maximum value when the bias is -15 V. When the bias voltage is less than 10 V, the 3-dB bandwidth is almost zero. When the bias voltage reaches V_p, the field strength is not high and the carrier drift speed is low which leads to small bandwidth. When the bias voltage

reaches the V_b, the 3-dB bandwidth becomes lower due to the limitation of gain bandwidth. It can be seen from Fig. 6 (a) that the actual measured maximum 3-dB bandwidth is 7.6 GHz. The calculated 3-dB bandwidth is 8.2 GHz. The difference may results from the fact that the parasitic capacitance and resistance are not be considered in the calculation. Figure. 6 (b) shows the 3-dB bandwidth against multiplication gain of the fabricated APD. The GBP can reach 155 GHz, which is consistent with the calculated results.

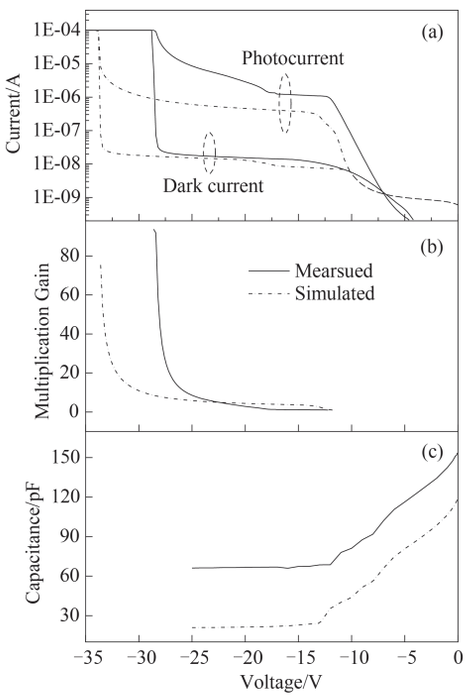

Fig. 4 (a) Measured and Calculated *I-V* characteristic, (b) multiplication gain vs voltage, and (c) *C-V* characteristic of the InAlAs/InGaAs APD
图4 (a) 器件的实际和计算电流-电压曲线,(b) 增益-电压关系曲线,(c) 电容-电压曲线

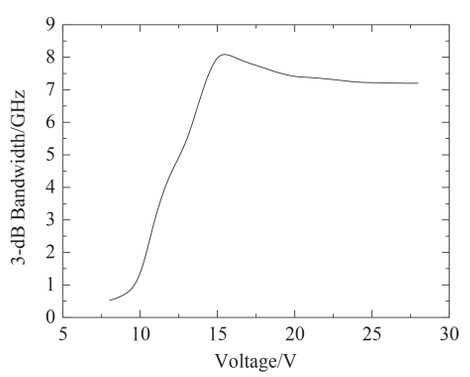

Fig. 5 3-dB bandwidth vs voltage
图5 3-dB带宽随偏压的变化曲线

4 Conclusion

In this paper, an InAlAs/InGaAs APD with SAGCM structure was designed. The quantitative and predictive physical model with the operation of the device was established. The fabricated device bandwidth was 7.6 GHz and the GBP reached 155 GHz while the dark current was only 19 nA (at 90% V_b). However, since the parameters adopted in the simulation are too ideal and the effect of the process of device fabrication on the device performance is not considered, the simulated results are far away from the experimental results. A real material parameter as well as a less effect of the device fabrication is needed in the following work. This study is significant to the future high-speed transmission application of the avalanche photodiodes.

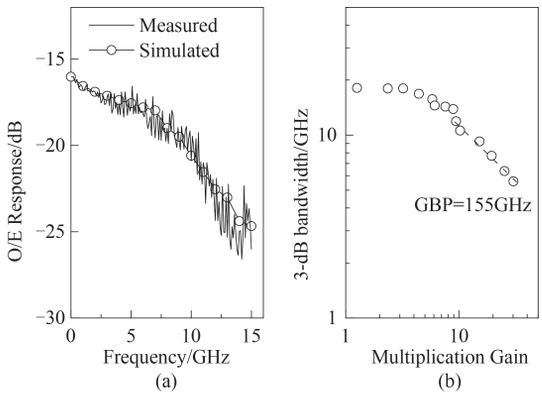

Fig. 6 (a) Measured and Calculated frequency characteristic, and (b) 3-dB bandwidth vs multiplication gain of fabricated InAlAs/InGaAs APD
图6 (a) 实际和计算的频率响应特性曲线,(b) 制备器件的3-dB带宽和增益关系曲线

Acknowledgment

The authors are thankful for the technical support from Nano Fabrication Facility, Platform for Characterization & Test of SINANO, CAS. Financial supports are given in the footnote on the first page.

References

[1] Campbell J C. Recent advances in avalanche photodiodes [J]. *Journal of Lightwave Technology*, 2016, **34**(2): 278-285.
[2] Nada M, Yoshimatsu T, Nakajima F, *et al*. A 42-GHz bandwidth avalanche photodiodes based on III-V compounds for 106-Gbit/s PAM4 applications [J]. *Journal of Lightwave Technology*, 2019, **37**(2): 260-265.
[3] Bertone N, Clark W. Avalanche photodiode arrays provide versatility in ultrasensitive applications [J]. *Laser Focus World*, 2007, **43**(9): 69.
[4] Mitra R, Beck J D, Skokan M R, *et al*. Intelligent Integrated Microsystems, 2006,6232.
[5] Meng X, Tan C H, Dimler S, *et al*. 1 550 nm InGaAs/InAlAs single photon avalanche diode at room temperature [J]. *Optics Express*, 2014, **22**(19): 22608-22615.
[6] Zhao K, You S, Cheng J, *et al*. Self-quenching and self-recovering InGaAs/InAlAs single photon avalanche detector [J]. *Applied Physics Letters*, 2008, **93**(15).
[7] LI Yong-Fu, LIU Jun-Liang, WANG Qing-Pu, *et al*. Avalanche characterization of high speed single-photon detector based on InGaAs/InP APD[J]. J.*Infrared Millim.Waves*(李永富, 刘俊良, 王青圃, 等。基于InGaAs/InP雪崩光电二极管的高速单光子探测器雪崩特性研究。**红外与毫米波学报**), 2015, **34**(4): 427-431.
[8] LI Bin, CHEN Wei, HUANG Xiao-Feng, *et al*. InP cap layer doping density in InGaAs/InP single-photon avalanche diode[J]. J.*Infrared Millim.Waves*(李彬, 陈伟, 黄晓峰, 等。InGaAs/InP单光子雪

崩光电二极管InP顶层掺杂研究。**红外与毫米波学报**), 2017, **36**(004): 420-424.
[9] Nakata T, Ishihara J, Makita K, *et al*. Multiplication noise characterization of InAlAs-APD with heterojunction [J]. *Ieee Photonics Technology Letters*, 2009, **21**(24): 1852-1854.
[10] Campbell J C. Recent advances in telecommunications avalanche photodiodes [J]. *Journal of Lightwave Technology*, 2007, **25**(1): 109-121.
[11] Nada M, Muramoto Y, Yokoyama H, *et al*. Inverted InAlAs/InGaAs avalanche photodiode with low-high-low electric field profile [J]. *Japanese Journal of Applied Physics*, 2012, **51**(2).
[12] Ferraro M S, Clark W R, Rabinovich W S, *et al*. InAlAs/InGaAs avalanche photodiode arrays for free space optical communication [J]. *Applied Optics*, 2015, **54**(31): F182-F188.
[13] Chen J, Zhang Z, Zhu M, *et al*. Optimization of InGaAs/InAlAs avalanche photodiodes [J]. *Nanoscale Research Letters*, 2017, 12.
[14] Parks J W, Brennan K E, Tarof L E. Macroscopic device simulation of InGaAs/InP based avalanche photodiodes [J]. *Vlsi Design*, 1998, **6**(1-4): 79-82.
[15] Watanabe I, Torikai T, Taguchi K. Monte-Carlo simulation of impact ionization rates in inalas-ingaas square and graded barrier superlattice [J]. *IEEE Journal of Quantum Electronics*, 1995, **31**(10): 1826-1834.
[16] Watanabe I, Torikai T, Makita K, *et al*. Impact ionization rates in (100) AL0.48IN0.52AS [J]. *IEEE Electron Device Letters*, 1990, **11**(10): 437-438.
[17] Parks J W, Brennan K F, Tarof L E J V D. Macroscopic device simulation of InGaAs/InP based avalanche photodiodes [J]. 2014, **6**(1-4): 79-82.
[18] Watanabe I, Torikai T, Taguchi K J I J o Q E. Monte Carlo simulation of impact ionization rates in InAlAs-InGaAs square and graded barrier superlattice [J]. 1995, **31**(10): 1826-1834.
[19] Matsushima Y, Sakai K, Noda Y J I E D L. New type InGaAs/InP heterostructure avalanche photodiode with buffer layer [J]. 2005, **2**(7): 179-181.
[20] Jiang X, Itzler M A, Ben-Michael R, *et al*. InGaAsP - InP Avalanche Photodiodes for Single Photon Detection [J]. 2007, **13**(4): 895-905.
[21] CHENG Yu-Shun, GUO Hui-Jun, LI Hao, *et al*. Device design pf planner PIN HgCdTe avalanche photodiode [J]. J. *Infrared Millim. Waves*(程雨顺, 郭慧君, 李浩, 等。碲镉汞APD平面型PIN结构仿真设计。**红外与毫米波学报**), 2020, **39**(1):8-14.